processes

MDPI

Article

Novel Magnetically-Recoverable Solid Acid Catalysts with a Hydrophobic Layer in Protecting the Active Sites from Water Poisoning

Jingjing Liu [1], Juanli Shi [2], Bo Zhang [3] and Zhenmin Cheng [1,*]

[1] State Key Laboratory of Chemical Engineering, School of Chemical Engineering, East China University of Science and Technology, Shanghai 200237, China
[2] China National Nuclear Industry Corporation 404, Jiayuguan 735100, China
[3] State Key Laboratory of Molecular Engineering of Polymers, Department of Macromolecular Science, Fudan University, Shanghai 200438, China
* Correspondence: zmcheng@ecust.edu.cn; Tel.: +86-21-6425-3529; Fax: +86-21-6425-3528

Abstract: Three novel magnetically-recoverable solid acid catalysts (hydrophobic catalysts Fe_3O_4@SiO_2-Me&$PrSO_3H$, Fe_3O_4@SiO_2-Oc&$PrSO_3H$ and hydrophilic catalyst Fe_3O_4@SiO_2-$PrSO_3H$) were synthesized by introducing organic propylsulfonic acid and alkyl groups to Fe_3O_4@SiO_2 nanocomposites. We characterized these catalysts by FT-IR, EDS, XRD, VSM and SEM, and found that they had excellent core-shell structure and magnetic responsiveness. We also explored the impact of surface hydrophobicity on activity and stability of catalysts in ethyl acetate (EAC) synthesis reaction. The results indicated that: for reactivity and reusability, Fe_3O_4@SiO_2-Oc&$PrSO_3H$ > Fe_3O_4@SiO_2-Me&$PrSO_3H$ > Fe_3O_4@SiO_2-$PrSO_3H$. This was because octyl and methyl groups could build a hydrophobic layer on the surfaces of Fe_3O_4@SiO_2-Oc&$PrSO_3H$ and Fe_3O_4@SiO_2-Me&$PrSO_3H$, and this could effectively prevent water molecules from poisoning active sites; the hydrophobicity of octyl was stronger than methyl. Fe_3O_4@SiO_2-Oc&$PrSO_3H$ also showed higher catalytic activity in the external aqueous reaction system, which indicated that it had good water toleration. Moreover, we could easily separate Fe_3O_4@SiO_2-Oc&$PrSO_3H$ from the reaction mixture with an external magnetic field, in the meanwhile, its reactivity could still remain above 80% after reusing 6 times.

Keywords: core-shell structured Fe_3O_4@SiO_2 support; hydrophobicity; esterification reaction; magnetically-recoverable solid acid catalysts

Citation: Liu, J.; Shi, J.; Zhang, B.; Cheng, Z. Novel Magnetically-Recoverable Solid Acid Catalysts with a Hydrophobic Layer in Protecting the Active Sites from Water Poisoning. *Processes* **2022**, *10*, 1738. https://doi.org/10.3390/pr10091738

Academic Editor: Zhenmeng Peng

Received: 7 August 2022
Accepted: 27 August 2022
Published: 1 September 2022

1. Introduction

In the past few decades, with people's increasing awareness of environmental protection and sustainable development, the concept of green chemistry came into being. Green chemistry advocates the replacement of hazardous reagents and products with reagents and products that have less impact on health [1], and revolves around waste recycling to achieve sustainable development [2]. As an important branch of green chemistry, green catalysis has attracted more and more attention from scientists seeking to develop novel and sustainable catalysts, and many creative research results have emerged. For example, Xu et al. [3] utilized one-pot method to synthesize photo-Fenton catalyst La-Fe-O@CN for efficient removal of organic dyes from wastewater. Zhang et al. [4] fabricated a hydrophobic zinc foam electrode by electrodeposition as the catalyst for the electroreduction of carbon dioxide (CO_2) to carbon monoxide (CO), which provided a new idea for the conversion and utilization of CO_2.

In the field of catalytic reactions, the development of solid catalysts with high activity, high target selectivity, reusability, mild reaction conditions and easy separation is very necessary. As one of the important catalytic reactions, the esterification reaction generally uses sulfuric acid (H_2SO_4) as the catalyst. However, these liquid acids as catalysts also

have defects such as harsh reaction conditions, corrosion of equipment, environmental pollution, and difficulty in subsequent separation [5], which are obviously not in line with the principles of green chemistry; hence many solid acid catalysts have been designed and synthesized by researchers to replace liquid acid catalysts [6]. For example, Shu et al. [7] synthesized a novel solid Brönsted–Lewis acid catalyst La-PW-SiO_2/SWCNTs by sol-gel method for synthesis of biodiesel by esterification of oleic acid and methanol, and Mani Durai et al. [8] supported phosphotungstic acid (PTA) on mesoporous Al-SBA-15 to synthesize the catalyst PTA/Al-SB, which exhibited up to 96% conversion rate of valeric acid and 100% selectivity of ethyl valerate in the esterification reaction of valeric acid and ethanol. Compared with liquid acids, solid acids exhibit higher reactivity and good reusability in esterification reactions [9,10], and they are less corrosive to facilities [11–15], while people can recover them from the reaction solution by simple separation methods [16,17]. However, most solid acid catalysts have a hydrophilic surface, and the water molecules produced by the esterification reaction will be adsorbed on the hydrophilic surface, leading to the leaching of the active components or collapse of the framework structure (Table 1), which ultimately affects the reaction activity and stability of the catalysts [5]. Constructing a hydrophobic layer on solid acid catalysts' surface can prevent water molecules from poisoning the active sites, thereby allowing the desired reaction to proceed. Thus, the preparation of hydrophobic solid acid catalysts has very important research significance for esterification reactions.

Table 1. Influence of water molecules on hydrophilic solid acid catalysts and the advantages of hydrophobic solid acid catalysts.

Hydrophilic Solid Acid Catalysts	Hydrophobic Solid Acid Catalysts
Occupying catalyst active sites	Improving catalytic performance of catalysts
Leaching of active components	Improving stability of catalysts in polar medium
Leading to the collapse of the framework structure	Enhancing working life of catalysts
Suppressing the progress of the forward reaction	Expanding applications in acid-catalyzed reactions

Nanoparticles have the characteristics of small size, large specific surface area and many active centers, so they are an excellent choice for solid acid catalyst supports. However, because of the small size, it is difficult to separate nano-catalysts by traditional filtration techniques [6], and the use of ultracentrifugation will greatly increase the time cost and economic cost, which greatly limits the application of nanoparticles in the catalysis industry. Researchers have used magnetic nanoparticles (MNPs) to overcome above problem. The insolubility and paramagnetism of MNPs allow the catalysts to be simply and efficiently separated from liquid reaction mixture by a magnet [18]. In addition, because inexpensive raw materials and simple synthetic methods can be used to prepare MNPs, and certain functions can be achieved by simple surface modification of them [19], the development of nanotechnology makes MNPs stand out in the fields of catalysis, sewage treatment, adsorbents, and biomedicine [20–22]. At the same time, MNPs are increasingly being developed through interdisciplinary research. S. Bhaskar et al. [23] integrated streptavidin magnetic nanoparticles (SMPNs) and graphene oxide π-plasmons as key spacer materials for augmented surface plasmon-coupled fluorescence (SPCF), obtaining ~500-fold of SPCF enhancement; SMPNs alone as spacer material also obtained ~100-fold SPCF enhancement. However, most of the MNPs are ferroferric oxide (Fe_3O_4), which are easily oxidized and prone to polymerize in the exposed chemical environment [24–26], hindering the application of MNPs as catalyst supports. Therefore, researchers usually used Stöber method and sol-gel method to coat the surface of MNPs with one or more layers of inert silicon dioxide (SiO_2) to solve the above problems [27,28]. Coating SiO_2 on the surface of Fe_3O_4 nanoparticles can synthesize core-shell structured Fe_3O_4@SiO_2 nanocomposites, and

they have the following advantages: (1) The inert SiO_2 shell can avoid the aggregation or oxidation of MNPs [25,29], and improve their chemical stability; (2) The SiO_2 shell can make MNPs more dispersed in polar solvents; (3) Magnetic nanocomposites with different structural characteristics can be prepared by adjusting the ratio of raw materials [30]; (4) The surface of the SiO_2 shell contains many -OH groups, which are easy to graft other active groups, and then improve the stability of MNPs and increase the number of catalysts' active sites [29].

Fe_3O_4@SiO_2 can be used as the support to prepare magnetically-recoverable solid acid catalysts. Researchers have introduced acidic substances or acidic groups into Fe_3O_4@SiO_2 magnetic nanocomposites to improve their catalytic activity, mainly including ionic liquids [31–33], heteropoly acids [34], -SO_3H groups [35], organic sulfonic acid groups [36,37], etc. However, despite there being many studies to synthesize and characterize acidic Fe_3O_4@SiO_2 nanomaterials, few researchers have combined hydrophobicity and acidity to provide bifunctional core-shell Fe_3O_4@SiO_2 nanomaterials [38]. It is a very challenging task to introduce both sulfonic groups and hydrophobic groups on the Fe_3O_4@SiO_2 surface. It requires not only the combination of acidity and hydrophobicity [39–41], but also the combination of inorganic supports and organic functional groups at the nanoscale. In addition, the introduction of hydrophobic groups on the acidic Fe_3O_4@SiO_2 nanomaterials can protect the catalysts from water poisoning in the aqueous reaction system, and enhance the stability and reactivity of the catalysts.

Therefore, combined with the superior properties of Fe_3O_4@SiO_2 and the current situation that solid acid catalysts are prone to deactivate due to water poisoning in the esterification reaction, we co-grafted propylsulfonic acid and hydrophobic alkyl groups on Fe_3O_4@SiO_2, and developed three novel, magnetically-recyclable, economical and environmentally friendly solid acid catalysts, and tested their practicability by EAC synthesis reaction. At the same time, we also explored the impact of the surface hydrophobicity on solid acid catalysts' reactivity and stability by comparing the catalytic activity and reusability of catalysts Fe_3O_4@SiO_2-$PrSO_3H$, Fe_3O_4@SiO_2-Me-$PrSO_3H$ and Fe_3O_4@SiO_2-Oc-$PrSO_3H$. In addition, to clearly demonstrate the advantages of hydrophobic solid acid catalysts in controlling the microenvironment around acid sites under harsh reaction conditions, we also performed the esterification reaction under the condition of artificially added water, and found that the hydrophobic modification of octyltriethoxysilane (OTS) greatly improved catalyst' stability and reactivity for synthesizing EAC in water. As far as we know, it is the first report demonstrating the high catalytic performance of propanesulfonic acid and alkyl groups co-fixed solid acid catalysts for EAC synthesis under excess water conditions.

2. Chemicals and Methods

2.1. Chemicals and Characterizations

Fe_3O_4 nanoparticles (20 nm, ShuiTian, Shanghai, China). Anhydrous ethanol (EtOH) and toluene (≥99.5%, Sinopharm Chemical Reagent, Shanghai, China). Ammonia solution (25–28%, Macklin, Shanghai, China). (3-Mercaptopropyl) triethoxysilane (MPTES, 98%, Naicheng, Shanghai, China). Methyltrimethoxysilane (MTMS, 98%, Aladdin, Shanghai, China). Tetraethyl orthosilicate (TEOS, 98%, Aladdin, Shanghai, China). OTS (AR, Aladdin, Shanghai, China). Hydrogen peroxide (H_2O_2) solution (≥30%, Titan, Shanghai, China). Concentrated H_2SO_4 solution (95–98%, Titan, Shanghai, China). Phenolphthalein (AR, Titan, Shanghai, China). Glacial acetic acid (HOAc, AR). Standard sodium hydroxide (NaOH) solution (0.1 M). All reagents were used without further purification.

The element composition and molecular structure of the samples were judged according to the absorption frequency of different functional groups to infrared light. A spectrum 100 infrared spectrometer was used to record FT-IR spectra with the potassium bromide (KBr) pellet method (scanning range: 400–4000 cm^{-1}). EDS spectra were measured on the FE-SEM ZeissGemin 300 (Carl Zeiss AG, Germany) to determine whether SiO_2 was successfully coated on Fe_3O_4 nanoparticles and whether propylsulfonic acid groups and

octyl groups were successfully introduced on Fe_3O_4@SiO_2 nanocomposites. The instrument was equipped with EDS spectrometer, Inlens and ET secondary electron detectors. Specific test conditions: First, use of EtOH to disperse the sample; then, sonication for 10 min and spraying gold; finally, shape detection and energy spectrum point scanning. XRD patterns were measured on a Polycrystalline/D8 Advance DaVinci X-ray diffractometer (Bruker AXS GmbH, Germany, 40.0 kV, 30.0 mA, Cu Kα radiation) to determine samples' crystal structure. The 2θ rotation range was 5°–80° with 2°/min scanning rate. VSM was detected by PPMS-9 vibrating sample magnetometer (Quantum Design, U.S.) to measure the samples' hysteresis loops (vacuum, room temperature, scanning range: −30,000–30,000 Oe). SEM test was carried out on a FE-SEM ZeissGemin 300 instrument (Carl Zeiss AG, Germany).

2.2. Preparation of Catalysts

2.2.1. Fe_3O_4@SiO_2 Supports

The preparation of Fe_3O_4@SiO_2 referred to the previous literatures [25,38]. The specific operational process was as follows: 2.0 g Fe_3O_4 nanoparticles and 400 mL EtOH were put into a three-necked flask, and the Fe_3O_4 was more uniformly dispersed in EtOH by an ultrasonic pre-mixing for 30 min (room temperature). Then, 12 mL ammonia solution (25–28%) was slowly added to the mixture and it was stirred at 40 °C for 30 min. The solution was heated to 60 °C, and 4 mL TEOS was added dropwise, after which the mixture was stirred at 60 °C for 24 h. Finally, the solid was magnetically separated and washed 3 times with EtOH, then dried under vacuum at 60 °C for 12 h to obtain silica-coated magnetic Fe_3O_4@SiO_2 nanocomposites.

2.2.2. Hydrophilic Catalyst Fe_3O_4@SiO_2-$PrSO_3H$

The preparation of Fe_3O_4@SiO_2-PrSH referred to the previous literature [37]. In a typical preparation procedure, 2.0 g Fe_3O_4@SiO_2, 30 mL toluene and 1.6 g MPTES were put into a three-necked flask and mixed well. The obtained solution was heated to reflux at 110 °C for 4 h. The solid was magnetically separated and washed with EtOH. Finally, it was dried under vacuum at 60 °C for 12 h to obtain solid Fe_3O_4@SiO_2-PrSH. The obtained solid Fe_3O_4@SiO_2-PrSH was oxidized by 30 wt% H_2O_2 solution (30 mL solution/g solid) and stirred for 12 h (room temperature). Then, H_2SO_4 solution (6 M) was added with a volume ratio of 2:1 to H_2O_2 solution and the mixture was stirred for another 12 h (room temperature). The solid was magnetically separated and washed 3 times with EtOH, then dried under vacuum at 60 °C for 12 h to obtain the catalyst Fe_3O_4@SiO_2-$PrSO_3H$.

2.2.3. Hydrophobic Catalysts Fe_3O_4@SiO_2-Oc&$PrSO_3H$ and Fe_3O_4@SiO_2-Me&$PrSO_3H$

The hydrophobic catalyst Fe_3O_4@SiO_2-Oc&$PrSO_3H$ was synthesized by the following process: 30 mL toluene, 1.5 g Fe_3O_4@SiO_2-PrSH and a certain amount of OTS solution (1 mL OTS/g solid) were put into a three-necked flask and mixed well. The obtained solution was heated to reflux at 110 °C for 24 h. The solid was then separated with a permanent magnet, washed with EtOH and dried under vacuum at 60 °C for 12 h to obtain solid Fe_3O_4@SiO_2-Oc&PrSH. Fe_3O_4@SiO_2-Oc&PrSH was oxidized by 30 wt% H_2O_2 solution (30 mL solution/g solid) and stirred for 12 h (room temperature). H_2SO_4 solution (6 M) was then added with a volume ratio of 2:1 to H_2O_2 solution and stirring continued for another 12 h (room temperature). The solid was then magnetically separated, washed 3 times with EtOH and dried under vacuum at 60 °C for 12 h to obtain Fe_3O_4@SiO_2-Oc&$PrSO_3H$. The preparation process of Fe_3O_4@SiO_2-Me&$PrSO_3H$ was the same as that of Fe_3O_4@SiO_2-Oc&$PrSO_3H$, except that OTS was replaced with MTMS. The flow chart of the preparation of the three catalysts is shown in Figure 1.

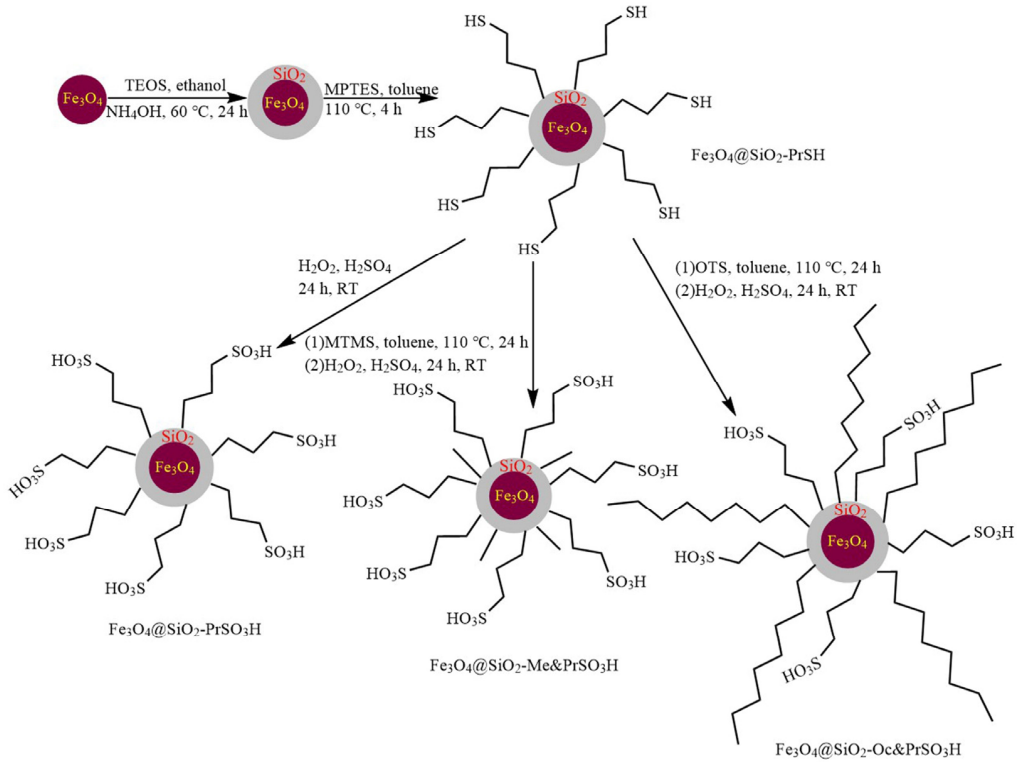

Figure 1. Preparation process of catalysts Fe_3O_4@SiO_2-$PrSO_3H$, Fe_3O_4@SiO_2-Me&$PrSO_3H$ and Fe_3O_4@SiO_2-Oc&$PrSO_3H$.

2.3. EAC Synthesis

We used the EAC synthesis reaction to test the stability and reactivity of the prepared catalysts. The reaction equation is shown in Formula (1) (note: CH_3COOH, CH_3CH_2OH, and $CH_3COOCH_2CH_3$ are the abbreviated structural formulas of acetic acid, ethanol, and ethyl acetate, respectively).

$$CH_3COOH + CH_3CH_2OH \overset{\text{catalysts}}{\rightleftharpoons} CH_3COOCH_2CH_3 + H_2O \quad (1)$$

We added a certain molar ratio of EtOH and HOAc, and a certain content of catalysts to a three-necked flask in sequence, assembled the experimental instruments and continued the reaction at 80 °C for some time. After the solution cooled to room temperature, we used a magnet to separate the catalysts from the reaction solution. We used a pipette to accurately take out 0.5 mL reaction solution and put it in a conical flask containing 20 mL of deionized water. We used 1% phenolphthalein and standard NaOH solution (0.1 M) for acid-base titration to determine the HOAc concentration C_1 after the reaction. Before the reaction, we had taken out 0.1 mL of the reaction solution for acid-base titration to determine the initial concentration C_0 of HOAc. Three samples were measured in parallel and the average value was taken. We calculated the conversion rate of HOAc according to Formula (2).

$$x = (1 - \frac{C_1}{C_0}) \times 100\% \quad (2)$$

x: the conversion rate of HOAc, %; C_0 and C_1, respectively, represented the concentration of HOAc before and after the reaction, M.

3. Results and Discussion

3.1. Catalysts' Hydrophilic and Hydrophobic Test

As far as we know, hydrophobic molecules tend to be non-polar and more easily dispersed in non-polar and neutral solutions (such as organic solvents). To investigate the hydrophilicity and hydrophobicity of the three functionalized catalysts, we dispersed them in a two-phase solvent system containing water and toluene [38], respectively. The test result showed that Fe_3O_4@SiO_2-$PrSO_3H$ nanoparticles were completely dispersed in the polar solvent water, while Fe_3O_4@SiO_2-Me&$PrSO_3H$ and Fe_3O_4@SiO_2-Oc&$PrSO_3H$ nanoparticles were completely dispersed in the non-polar solvent toluene (Figure 2). The result suggested that the higher hydrophobicity of Fe_3O_4@SiO_2-Me&$PrSO_3H$ and Fe_3O_4@SiO_2-Oc&$PrSO_3H$ compared to Fe_3O_4@SiO_2-$PrSO_3H$ could improve the catalysts' reactivity and stability in the water production reaction system.

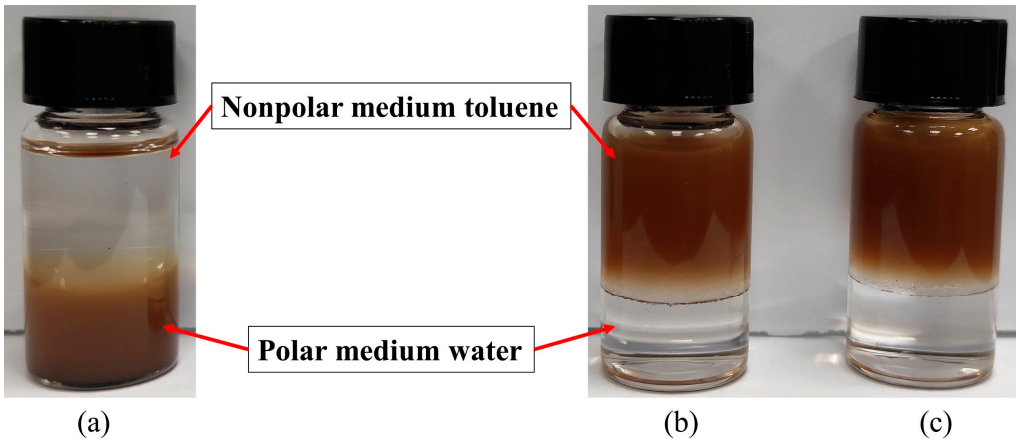

Figure 2. Macro picture for dispersion of (**a**) Fe_3O_4@SiO_2-$PrSO_3H$, (**b**) Fe_3O_4@SiO_2-Me&$PrSO_3H$ and (**c**) Fe_3O_4@SiO_2-Oc&$PrSO_3H$ in water and toluene two-phase system.

3.2. Catalyst Characterization

3.2.1. FT-IR

The FT-IR spectra of Fe_3O_4, Fe_3O_4@SiO_2, Fe_3O_4@SiO_2-$PrSO_3H$ and Fe_3O_4@SiO_2-Oc&$PrSO_3H$ were exhibited in Figure 3. In order to more directly observe the types of functional groups, we summarized all the absorption peak positions and types in Table 2. It could be seen that the typical infrared absorption peak of Fe_3O_4 appeared in all samples (υ (Fe-O)), and the absorption peaks of SiO_2 shell appeared in the FT-IR spectra of Fe_3O_4@SiO_2, Fe_3O_4@SiO_2-$PrSO_3H$ and Fe_3O_4@SiO_2-Oc&$PrSO_3H$ (δ (Si-O-Si), υ_s (Si-O-Si), υ_{as} (Si-O-Si) and υ (Si-OH)), which proved that the surface of Fe_3O_4 had been successfully coated with a layer of SiO_2. The absorption peak of propylsulfonic acid appeared in the FT-IR spectra of Fe_3O_4@SiO_2-$PrSO_3H$ and Fe_3O_4@SiO_2-Oc&$PrSO_3H$ (υ (O=S=O)), and the absorption peak of alkyl groups appeared in the FT-IR spectrum of Fe_3O_4@SiO_2-Oc&$PrSO_3H$ (υ (C-H)), which proved that propylsulfonic acid and alkyl groups had been successfully grafted on the surface of Fe_3O_4@SiO_2. It should be noted that since KBr would inevitably absorb water during sample preparation, the absorption peak of free or adsorbed water molecules also appeared in Figure 3 (υ (-OH of water)).

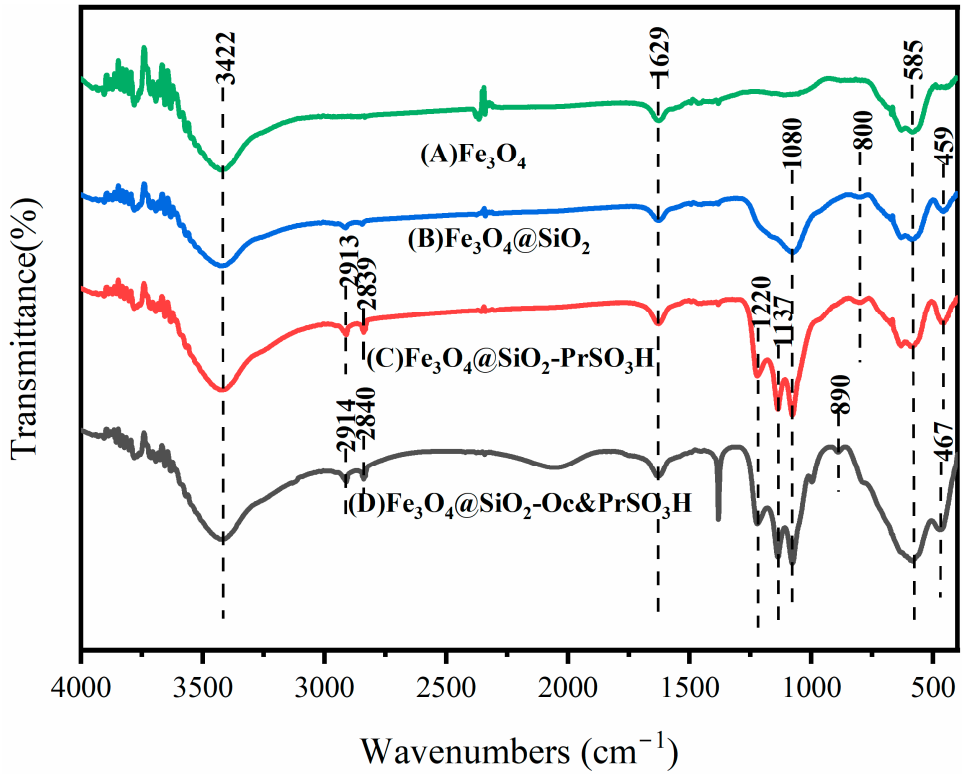

Figure 3. FT-IR spectra for (**A**) Fe_3O_4, (**B**) Fe_3O_4@SiO_2, (**C**)Fe_3O_4@SiO_2-$PrSO_3H$ and (**D**) Fe_3O_4@SiO_2-Oc&$PrSO_3H$.

Table 2. The analysis of FT-IR spectra of Fe_3O_4, Fe_3O_4@SiO_2, Fe_3O_4@SiO_2-$PrSO_3H$ and Fe_3O_4@SiO_2-Oc&$PrSO_3H$.

Samples / Peak Types	Fe_3O_4	Fe_3O_4@SiO_2	Fe_3O_4@SiO_2-$PrSO_3H$	Fe_3O_4@SiO_2-Oc&$PrSO_3H$
δ (Si-O-Si) [33]	-	459 cm^{-1}	459 cm^{-1}	467 cm^{-1}
υ (Fe-O) [33,42,43]	585 cm^{-1}	585 cm^{-1}	585 cm^{-1}	585 cm^{-1}
$υ_s$ (Si-O-Si) [37]	-	800 cm^{-1}	800 cm^{-1}	-
$υ_{as}$ (Si-O-Si) [38]	-	1080 cm^{-1}	1080 cm^{-1}	1080 cm^{-1}
υ (O=S=O) [44]	-	-	1137 and 1220 cm^{-1}	1137 and 1220 cm^{-1}
υ (-OH of water) [45]	1629 and 3422 cm^{-1}	1629 and 3422 cm^{-1}	1629 and 3422 cm^{-1}	1629 and 3422 cm^{-1}
υ (C-H) [38]	-	-	2839 and 2913 cm^{-1}	2840 and 2914 cm^{-1}
υ (Si-OH) [37]	-	3422 cm^{-1}	3422 cm^{-1}	3422 cm^{-1}

δ: bending vibration, υ: stretching vibration, $υ_s$: symmetric stretching vibration, $υ_{as}$: antisymmetric stretching vibration.

3.2.2. EDS

The EDS spectra of Fe_3O_4@SiO_2 support and catalyst Fe_3O_4@SiO_2-Oc&$PrSO_3H$ were displayed in Figure 4. Fe_3O_4@SiO_2 nanocomposites contained elements C (1.15 wt%), O (29.37 wt%), Fe (32.87 wt%), Si (36.61 wt%). Such a high content of Si could prove that the surface of Fe_3O_4 nanoparticles had been coated with a layer of SiO_2. The hydrophobic catalyst Fe_3O_4@SiO_2-Oc&$PrSO_3H$ contained the elements C (6.56 wt%), O (28.50 wt%), Fe (31.10 wt%), Si (32.48 wt%), S (1.36 wt%). After grafting propylsulfonic acid groups and octyl groups, the content of C and S elements increased significantly. By contrast, the content of O and Fe slightly decreased, which meant that propylsulfonic acid groups and octyl groups had been successfully immobilized on Fe_3O_4@SiO_2 support and was consistent with the results of FT-IR spectra.

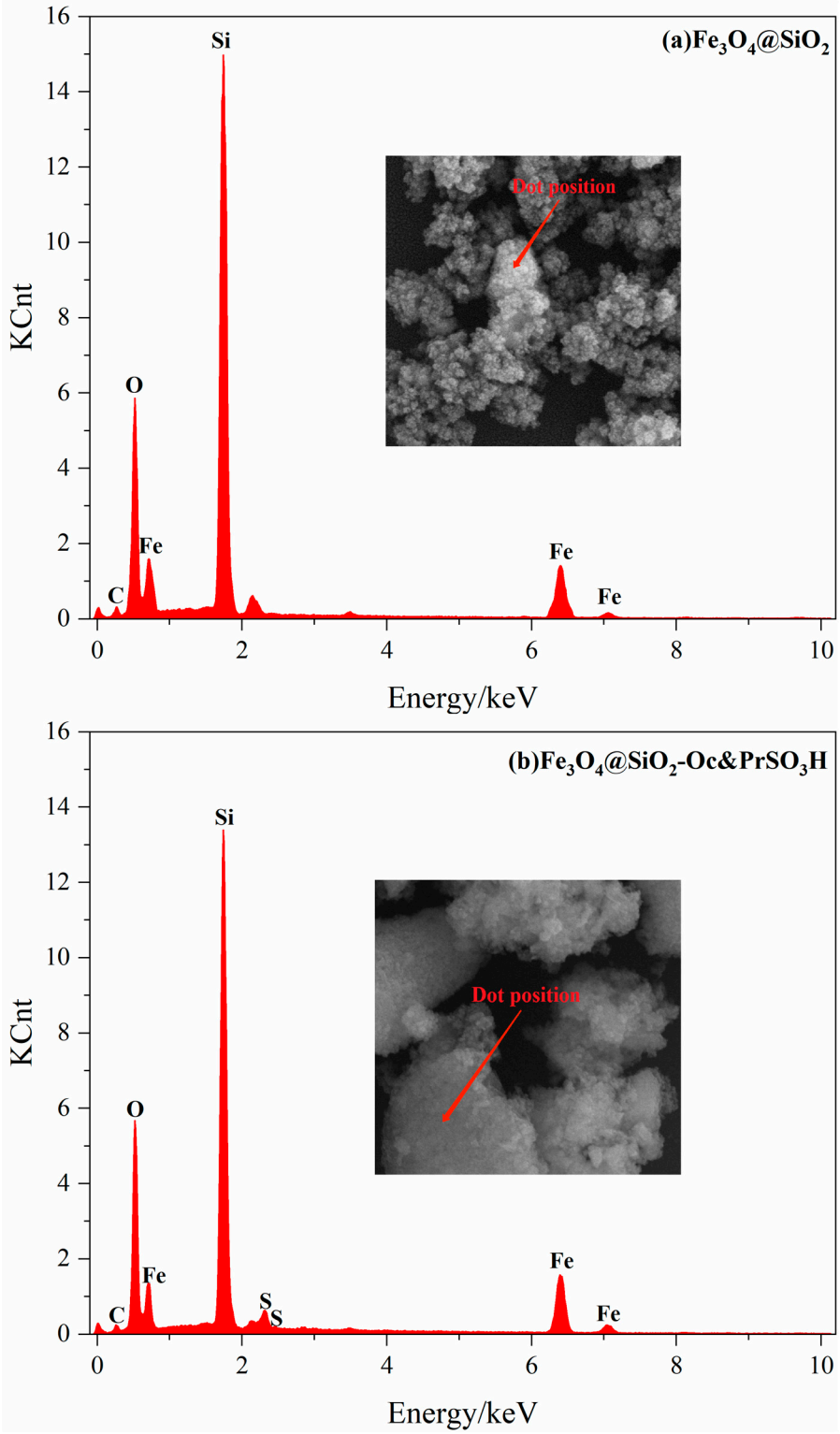

Figure 4. EDS spectra of (**a**) Fe_3O_4@SiO_2 and (**b**) Fe_3O_4@SiO_2-Oc&$PrSO_3H$; insert was dot position.

3.2.3. XRD

The wide-angle XRD spectra of Fe_3O_4 nanoparticles, Fe_3O_4@SiO_2 support, catalysts Fe_3O_4@SiO_2-$PrSO_3H$ and Fe_3O_4@SiO_2-Oc&$PrSO_3H$ are displayed in Figure 5. To our satisfaction, all samples showed diffraction peaks at 2θ = 30.16°, 35.52°, 43.17°, 53.56°, 57.10°, 62.70°, 74.19°, corresponding to typical reflection of the Fe_3O_4 crystal planes (220), (311), (400), (422), (511), (440) and (533). These values were very compatible with the

standard XRD pattern of Fe_3O_4 (PDF file NO. 88-0315). In addition, the weak broad band (2θ = 10°–20°) diffraction peaks appearing in Figure 5b–d could be ascribed to the amorphous SiO_2 shell on the surface of Fe_3O_4 core [46]. These results all indicated that Fe_3O_4 nanoparticles' crystal structure was well preserved during the functionalization process, which was beneficial to the magnetic separation of samples [32] and was consistent with the results of FT-IR and EDS. As we expected, from the comparison of Figure 5c,d and Figure 5a,b, we found that the XRD spectra of the organic-inorganic catalysts Fe_3O_4@SiO_2-$PrSO_3H$, Fe_3O_4@SiO_2-Oc&$PrSO_3H$ and the inorganic support Fe_3O_4@SiO_2 were not very different; this is because the organic groups grafted on the surface of Fe_3O_4@SiO_2 do not have any crystal structure [38]. In addition, Figure 5d showed that the crystal structure of the Fe_3O_4@SiO_2 support remained unchanged despite being modified by organic precursors. The crystallite size of catalyst Fe_3O_4@SiO_2-Oc&$PrSO_3H$ was estimated to be 27.52 nm using the Scherrer's equation.

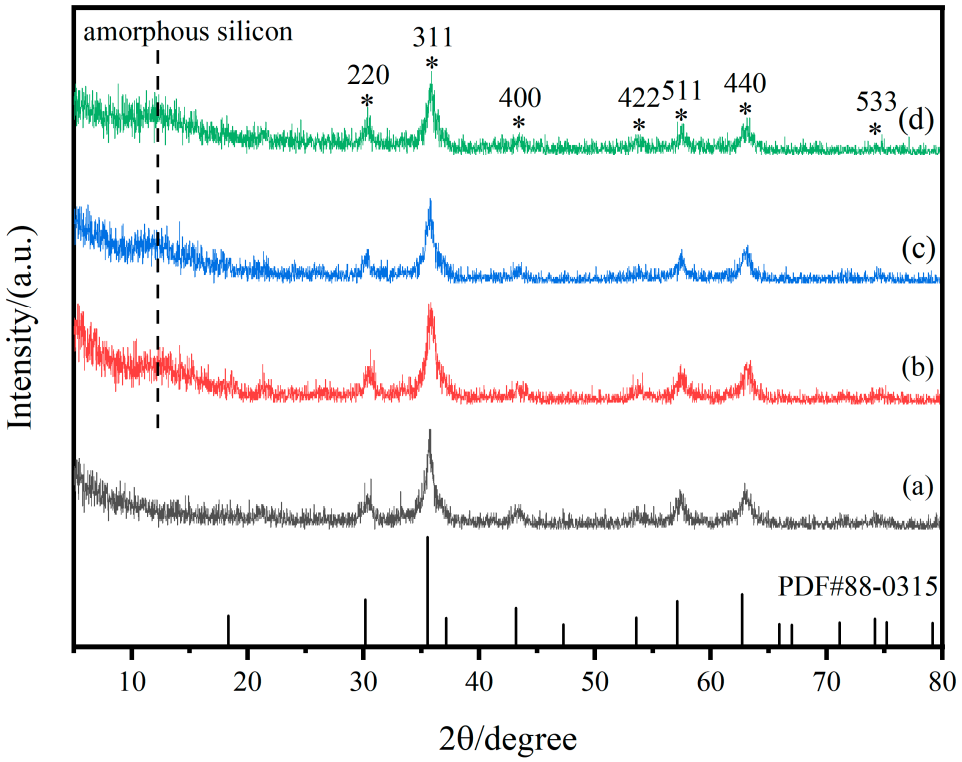

Figure 5. Wide-angle XRD spectra of (**a**) Fe_3O_4, (**b**) Fe_3O_4@SiO_2, (**c**) Fe_3O_4@SiO_2-$PrSO_3H$ and (**d**) Fe_3O_4@SiO_2-Oc&$PrSO_3H$ ("*" represents the position of the diffraction peak).

3.2.4. VSM

The hysteresis loops of Fe_3O_4 nanoparticles, Fe_3O_4@SiO_2 support, catalyst Fe_3O_4@SiO_2-Oc&$PrSO_3H$ are shown in Figure 6a. We found that all samples had no coercivity and remanence, and they exhibited superparamagnetic behavior [34,47]. The saturation magnetization value of the Fe_3O_4@SiO_2 support (46.25 emu/g) was lower than that of bare Fe_3O_4 nanoparticles (57.54 emu/g), which was due to the coating of Fe_3O_4 nanoparticles with a layer of SiO_2 [38]. The Fe_3O_4@SiO_2-Oc&$PrSO_3H$ had the lowest saturation magnetization of 42.81 emu/g. This was due to the grafting of non-magnetic octyl and propylsulfonic acid groups, and the result was consistent with other characterization results. Although the saturation magnetization of Fe_3O_4@SiO_2-Oc&$PrSO_3H$ was the lowest among the samples, it could be seen that the catalyst Fe_3O_4@SiO_2-Oc&$PrSO_3H$ could be easily separated by an external magnet without filtration or centrifugation (Figure 6b).

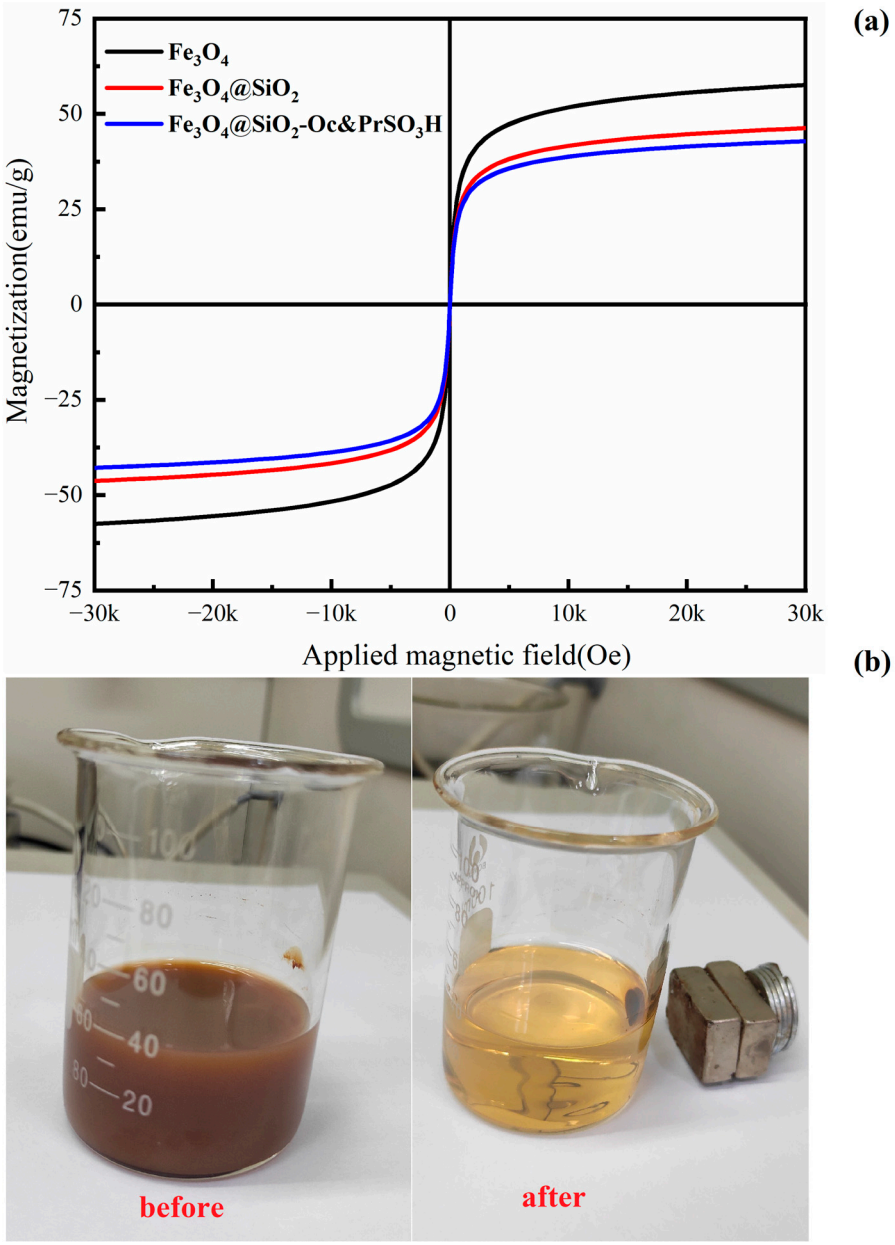

Figure 6. (**a**) The magnetic hysteresis loops of Fe_3O_4 nanoparticles, Fe_3O_4@SiO_2 support, catalyst Fe_3O_4@SiO_2-Oc&$PrSO_3H$; (**b**) Separation process of catalyst Fe_3O_4@SiO_2-Oc&$PrSO_3H$ from the reaction solution with an external magnet.

3.2.5. SEM

SEM test was carried out to obtain the morphology and average particle size of catalyst Fe_3O_4@SiO_2-Oc&$PrSO_3H$, and the results are shown in Figure 7. It can be seen that many catalyst particles agglomerated together to form floccules with irregular shapes. In addition, the surface of these catalyst particles was non-smooth, thus increasing the surface area. 200 particles were randomly selected on the SEM image and the size of each particle was measured. The particle size distribution was about 14–46 nm, and the average particle size was 29.52 ± 6.01 nm, which was in good agreement with the crystallite size of the catalyst Fe_3O_4@SiO_2-Oc&$PrSO_3H$ in the XRD pattern (27.52 nm). The particle size of the raw material Fe_3O_4 nanoparticles was 20 nm, so the thickness of the SiO_2 shell was about 4.8 nm.

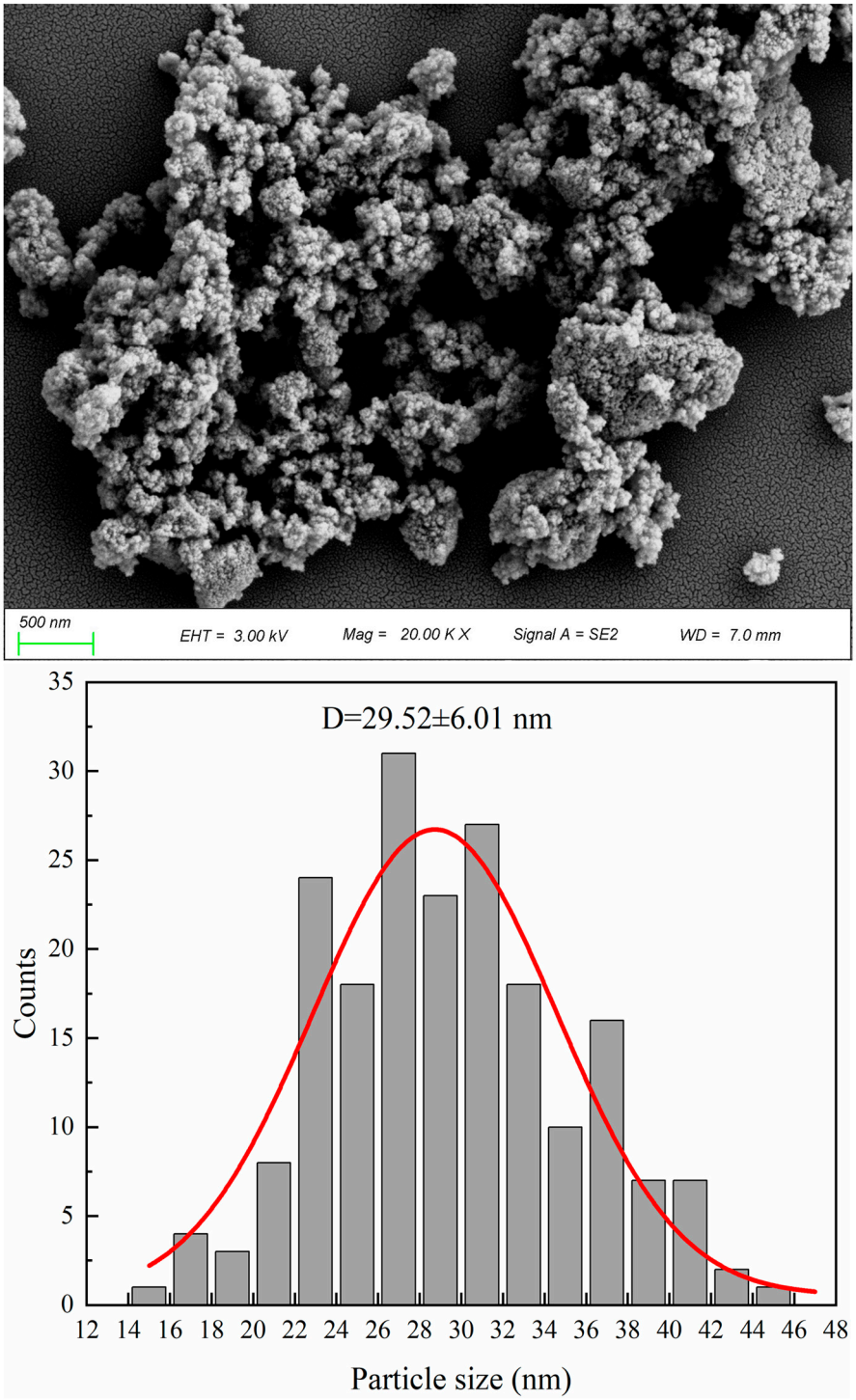

Figure 7. SEM image and particle size distribution of catalyst Fe_3O_4@SiO_2-Oc&PrSO_3H.

3.3. The Impact of the Molar Ratio of EtOH and HOAc on the Conversion Rate of HOAc

In the esterification reaction, we can increase the concentration of EtOH or HOAc to improve the yield of EAC, but in order to save production costs, the cheaper reactant is usually overused [48]. In this study, all corresponding alcohols were used in excess. 0.5359 g catalyst Fe_3O_4@SiO_2-Oc&PrSO_3H, 0.1 mol HOAc and some EtOH were put into a three-necked flask, the solution was heated to 80 °C and continued to react for 3 h. The changes of HOAc conversion rate when the amount of EtOH was respectively 0.2 mol, 0.3 mol, 0.4 mol, 0.5 mol, 0.6 mol and 0.7 mol were investigated, and the experimental results were shown in Figure 8. We found that when the molar ratio of EtOH to HOAc

increased, the conversion of HOAc also increased gradually. The HOAc conversion rate reached the maximum of 88.57% when the molar ratio of EtOH to HOAc was 6:1.

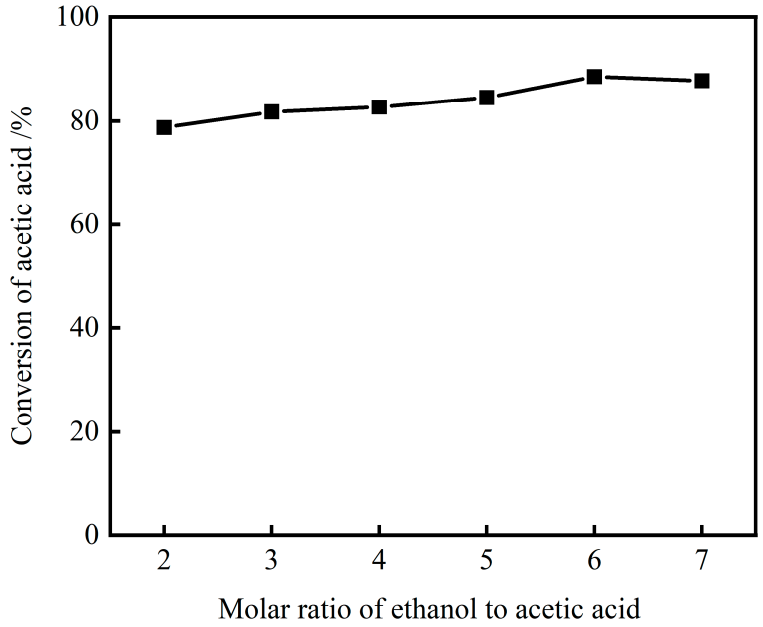

Figure 8. The impact of molar ratio of EtOH to HOAc on the conversion rate of HOAc (reaction conditions: 0.5359 g catalyst loading, 80 °C, 3 h, 640 rpm).

3.4. The Influence of the Amount of Catalyst on Reaction

We put 0.1 mol of HOAc, 0.6 mol of EtOH and a certain content of catalyst Fe_3O_4@SiO_2-Oc&PrSO_3H (accounting for the total mass fraction of the reactants) into a three-necked flask. The reaction was carried out at 80 °C for 3 h, and the effect of catalyst loading on the reaction was investigated. The results showed that as catalyst loading increased, the conversion rate of HOAc exhibited a trend of first increasing and then decreasing. When the catalyst loading was 1 wt%, the conversion rate of HOAc reached the maximum of 88.57% (Figure 9).

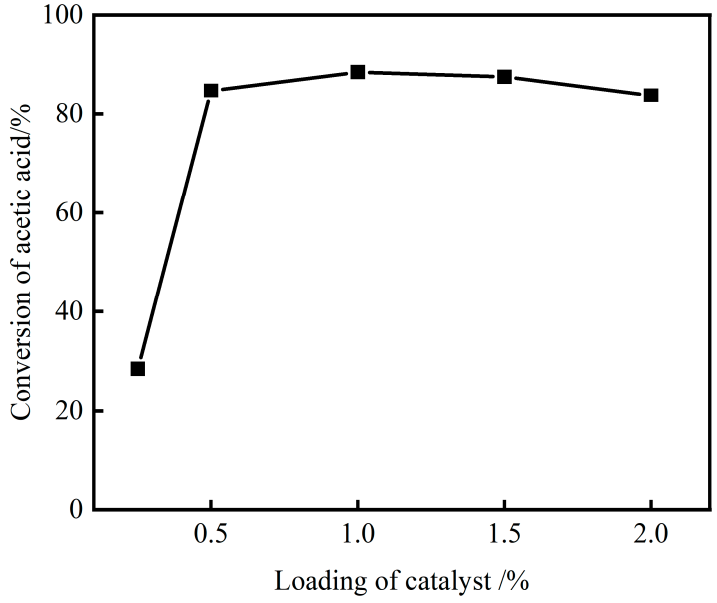

Figure 9. The effect of catalyst loading on the conversion rate of HOAc (reaction conditions: n_{EtOH}:n_{HOAc} = 6:1, 80 °C, 3 h, 640 rpm).

3.5. The Effect of Reaction Time on the Conversion Rate of HOAc

We mixed 0.1 mol HOAc, 0.6 mol EtOH and 1 wt% catalyst Fe_3O_4@SiO_2-Oc&$PrSO_3H$, and reacted them for a period of time at 80 °C to investigate the effect of reaction time on the conversion rate of HOAc. The experimental results are shown in Figure 10. It was found that the conversion rate of HOAc gradually increased with the increase of reaction time, and then tended to equilibrium. After 3 h of reaction, the conversion rate of HOAc reached the maximum of 88.57%.

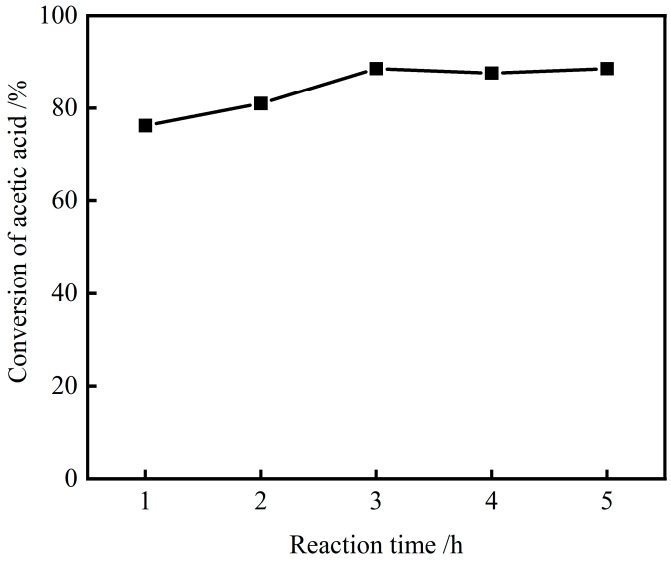

Figure 10. The influence of reaction time on the conversion rate of HOAc (reaction conditions: n_{EtOH}:n_{HOAc} = 6:1, 1 wt% catalyst loading, 80 °C, 640 rpm).

Through the above analysis, we could determine the optimal conditions for the EAC synthesis reaction: n_{EtOH}:n_{HOAc} = 6:1, 1 wt% catalyst loading, 80 °C, 3 h and 640 rpm, and the conversion rate of HOAc up to 88.57%.

3.6. Effect of Catalysts' Hydrophobicity on the Conversion Rate of HOAc and Reaction Rate

The reactivity of various catalysts in the EAC synthesis reaction is shown in Table 3. We found that the equilibrium conversion rate with the two hydrophobic catalysts Fe_3O_4@SiO_2-Me&$PrSO_3H$ and Fe_3O_4@SiO_2-Oc&$PrSO_3H$ were both higher than the hydrophilic catalyst Fe_3O_4@SiO_2-$PrSO_3H$; most importantly, the most hydrophobic Fe_3O_4@SiO_2-Oc&$PrSO_3H$ had the highest equilibrium conversion rate. Since the esterification reaction is reversible and limited by thermodynamic equilibrium, the surface hydrophobicity of the catalyst promotes the desorption of by-product water molecules and the enrichment of reactants, and promotes the shift of the equilibrium to the forward reaction direction [6,49], thus improving the equilibrium conversion rate of HOAc. To evaluate the intrinsic reactivity of the catalyst, we calculated the turnover frequency (TOF) of the reaction. We could see that the turnover frequency increased with the conversion rate, and Fe_3O_4@SiO_2-Oc&$PrSO_3H$ had the highest TOF value, indicated it had the fastest reaction kinetics [6]. This result shows that the catalyst surface hydrophobicity can not only accelerate the adsorption rate of reactants and the desorption rate of products, and promote the rapid progress of the esterification reaction, but also can protect the active components of the catalyst from leaching and avoid the reduction in reaction rate caused by the presence of by-product water molecules, thereby increasing HOAc conversion.

Table 3. Activity of catalysts in synthesis of EAC [a].

Samples	Catalysts	Conversion (%)	TOF [b] (h^{-1})
1	Fe_3O_4@SiO_2-$PrSO_3H$	85.71	5.098
2	Fe_3O_4@SiO_2-Me&$PrSO_3H$	87.62	5.212
3	Fe_3O_4@SiO_2-Oc&$PrSO_3H$	88.57	5.269

[a] Reaction conditions: n_{EtOH}:n_{HOAc} = 6:1, 1 wt% catalyst loading, 80 °C, 3 h, 640 rpm. [b] TOF = (M_{HOAc} × X)/($M_{catalyst}$ × t), M_{HOAc}, $M_{catalyst}$: the amounts of HOAc and catalysts; X: conversion of HOAc; t: reaction time.

3.7. The Influence of Water Content on Catalysts' Stability

The water molecules produced by the esterification reaction will be adsorbed on the surface of the catalysts, causing the loss of active components or the collapse of the framework structure, which will affect the stability and reactivity of the catalysts. Therefore, under the same reaction conditions, we added a certain volume fraction of water to the reaction system (2.5 vol.%, 5.0 vol.%, 7.5 vol.%, 10.0 vol.%, accounting for the total volume fraction of reactants) to detect the water resistance of the catalysts Fe_3O_4@SiO_2-$PrSO_3H$ and Fe_3O_4@SiO_2-Oc&$PrSO_3H$ [50,51], and then judged the influence of the octyl groups on the catalysts' water resistance. The experimental results are shown in Figure 11. It was found that the catalysts' activity was affected by the water content and the catalysts' composition. Water content had a more significant effect on the activity of the hydrophilic catalyst Fe_3O_4@SiO_2-$PrSO_3H$: when the water content was 2.5 vol.%, the HOAc conversion rate rapidly decreased by 8.0%. For the hydrophobic catalyst Fe_3O_4@SiO_2-Oc&$PrSO_3H$, the HOAc conversion rate was slightly reduced but remained above 85%. When the water content was further increased to 7.5 vol.%, the reaction activity of the hydrophilic catalyst Fe_3O_4@SiO_2-$PrSO_3H$ was reduced by 18.00%, while the reaction activity of the hydrophobic catalyst Fe_3O_4@SiO_2-Oc&$PrSO_3H$ was only reduced by 10.88%. Therefore, the introduction of octyl groups on the surface of Fe_3O_4@SiO_2-$PrSO_3H$ can form a hydrophobic area, which prevents water molecules from poisoning the active groups. In addition, the hydrophobic environment can separate the by-product water molecules from the reaction system in time, and promote the reaction in the direction of generating ethyl acetate, and thereby increase the conversion rate of HOAc [6].

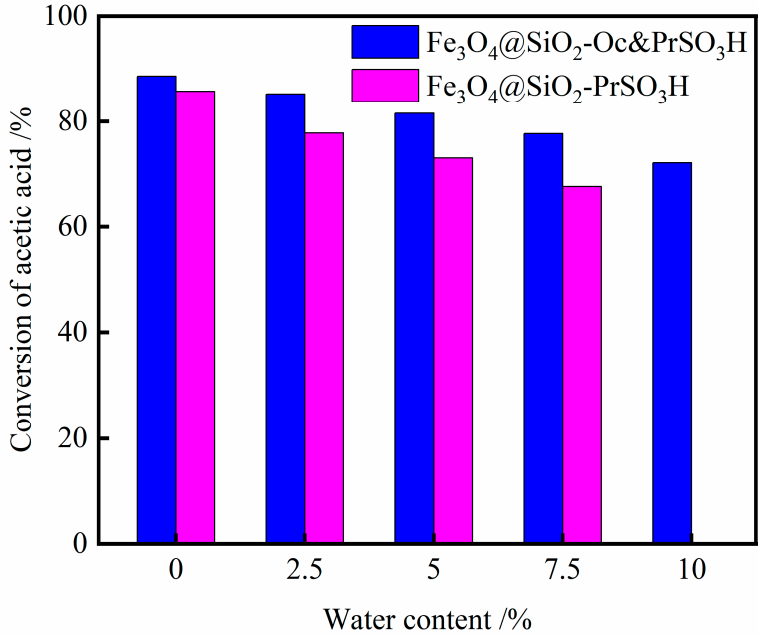

Figure 11. The influence of water content on esterification (reaction conditions: n_{EtOH}:n_{HOAc} = 6:1, 1 wt% catalyst loading, 80 °C, 3 h, 640 rpm).

The results suggested that: compared with hydrophilic catalyst Fe_3O_4@SiO_2-$PrSO_3H$, the hydrophobic environment on the surface of Fe_3O_4@SiO_2-Oc&$PrSO_3H$ not only improved its resistance to water molecules, but also enhanced the mass transfer process of the reactants, which led to the increase of HOAc conversion [38] (Figure 12).

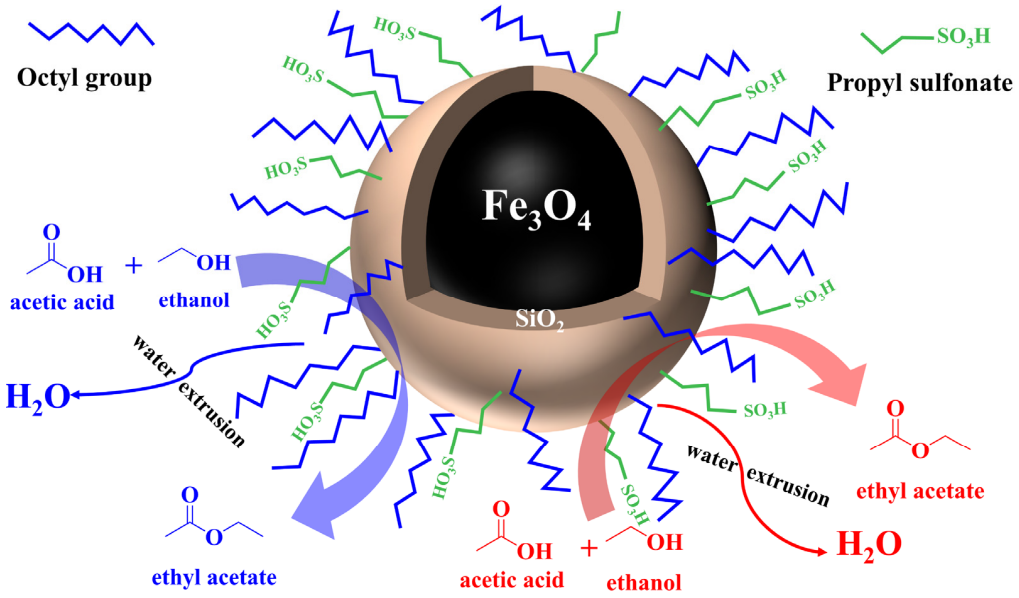

Figure 12. The reaction process of esterification on the surface of catalyst Fe_3O_4@SiO_2-Oc&$PrSO_3H$.

3.8. Reusability Test

We can evaluate the economic value and practical significance of catalysts by reusability [24], which is a vital factor for evaluating the performance of the catalyst in actual use. High reusability catalysts not only reduce the production cost of the catalyst, but also reduce the cost of synthesis of the EAC. Therefore, under the same reaction conditions, we investigated the reusability of catalysts Fe_3O_4@SiO_2-$PrSO_3H$, Fe_3O_4@SiO_2-Me&$PrSO_3H$, Fe_3O_4@SiO_2-Oc&$PrSO_3H$ to determine the impact of the solid acid catalysts surface wettability to reusability. The test method was as follows: when the reaction was completed, the magnetically separated catalyst was placed in 20 mL of EtOH and stirred for 30 min (room temperature) to remove the EAC and unreacted reactants adsorbed on the surface of the catalysts. The catalyst was magnetically separated, and again washed with 10 mL of EtOH. Finally, the obtained catalyst was dried under vacuum at 60 °C for 12 h. After drying, it was ensured that the same reaction conditions were used to restart the esterification reaction (note: we supplemented fresh catalysts to ensure the same amounts of catalysts for each repeated experiment).

The experimental results are shown in Figure 13. It can be seen that the catalyst Fe_3O_4@SiO_2-Oc&$PrSO_3H$ exhibited the highest reactivity and reusability, followed by Fe_3O_4@SiO_2-Me&$PrSO_3H$, and that Fe_3O_4@SiO_2-$PrSO_3H$ was the lowest. The reusability test showed that the activity of the catalyst Fe_3O_4@SiO_2-Oc&$PrSO_3H$ was slightly reduced by 0.95% after reusing 3 times, while after the catalysts Fe_3O_4@SiO_2-Me&$PrSO_3H$ and Fe_3O_4@SiO_2-$PrSO_3H$ were used repeatedly for three times, their activity was respectively reduced by 8.6% and 40.0%. The important thing was that the activity of Fe_3O_4@SiO_2-Oc&$PrSO_3H$ was still maintained above 80% after repeating its use 6 times, indicating that it had good reusability. Although these three catalysts contained the same amount of propylsulfonic acid groups, they exhibited different catalytic activity and reusability, mainly because the catalysts had different hydrophobicity. The surface of the catalysts Fe_3O_4@SiO_2-Oc&$PrSO_3H$ and Fe_3O_4@SiO_2-Me&$PrSO_3H$ contain hydrophobic octyl and methyl groups (Figure 1). On the one hand, the hydrophobic groups can expel water molecules from the reaction system in time and promote the conversion of HOAc; on the other hand, the hydrophobic surface prevents water molecules from being adsorbed on

the catalytic active sites and avoids water molecules from poisoning the catalyst, thereby improving the stability of the catalyst. In contrast, there are abundant hydrophilic sulfonic acid groups on the surface of the catalyst Fe_3O_4@SiO_2-$PrSO_3H$, and by-product water molecules will be adsorbed on the surface of the catalyst. On the one hand, they occupy the acid sites and hinder the transfer of reactants to the active sites, thereby suppressing the conversion of HOAc; on the other hand, the long-term adsorption of water molecules will cause the leaching of the active component -SO_3H groups, which will reduce the reusability and reactivity of the catalysts. Thus, the surface hydrophobicity of the catalysts has great effects on improving the reactivity and stability.

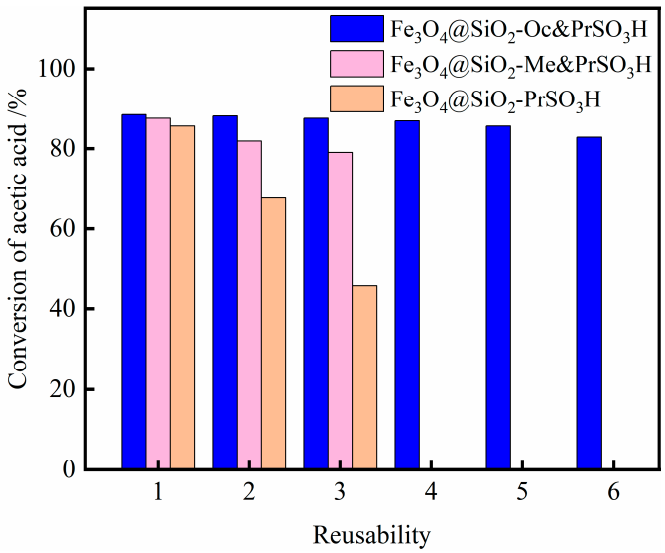

Figure 13. Reusability of catalysts Fe_3O_4@SiO_2-$PrSO_3H$, Fe_3O_4@SiO_2-Me&$PrSO_3H$, and Fe_3O_4@SiO_2-Oc&$PrSO_3H$ (reaction conditions: n_{EtOH}:n_{HOAc} = 6:1, 1 wt% catalyst loading, 80 °C, 3 h, 640 rpm).

We can also explain the phenomenon that the catalyst Fe_3O_4@SiO_2-Oc&$PrSO_3H$ has the highest reactivity and reusability by the comparison of molecular length. The propylsulfonic acid groups of the hydrophilic catalyst Fe_3O_4@SiO_2-$PrSO_3H$ (Figure 14a) are completely exposed to the water-producing reaction system because of the lack of hydrophobic groups protection, so water molecules can easily access these exposed propylsulfonic acid groups. This leads to the leaching of active components or the collapse of the framework structure, thereby reducing the catalytic effect and stability of the catalyst. Hence, its catalytic efficiency is significantly reduced during the recycling process. For the catalyst Fe_3O_4@SiO_2-Me&$PrSO_3H$ (Figure 14b), although it has a certain hydrophobic effect compared with Fe_3O_4@SiO_2-$PrSO_3H$, the length of the methyl is much shorter than propylsulfonic acid group, and its reactivity and reusability stability are also relatively poor. In contrast, the molecular length of the octyl groups dispersed on the surface of Fe_3O_4@SiO_2-Oc&$PrSO_3H$ is longer than propylsulfonic acid groups, and the hydrophobic environment caused by octyl groups will form a protective layer to protect the active components sulfonic acid groups from being leached [36], thereby significantly improving catalysts' reactivity and reusability. These results show that the catalyst Fe_3O_4@SiO_2-Oc&$PrSO_3H$ had a superior hydrophilic-hydrophobic and acidity balance in the water production reaction, which meant that it could still maintain more than 80% of the catalytic activity after reusing it 6 times.

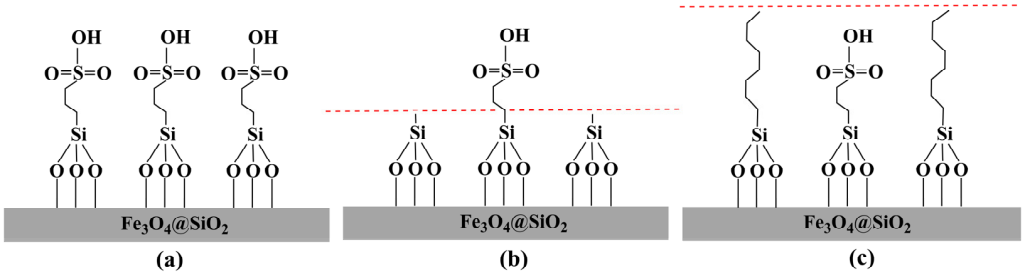

Figure 14. Comparison of the molecular length of propylsulfonic acid, methyl and octyl. (**a**) Fe_3O_4@SiO_2-$PrSO_3H$, (**b**) Fe_3O_4@SiO_2-Me&$PrSO_3H$ and (**c**) Fe_3O_4@SiO_2-Oc&$PrSO_3H$.

3.9. Comparison with Other Studies

To demonstrate the difference between the results of this work and other references, Table 4 summarized the catalytic evaluation data of different catalysts for the esterification of HOAc and alcohols. It could be seen that H_2SO_4 had high catalytic activity as the homogeneous catalyst [52], but it had the defects of many by-products, notably, difficult separation, corrosion of equipment and environmental pollution. Homogeneous catalyst hydrogen iodide had the same problems as H_2SO_4, and its catalytic performance was very low, at only 53.13% [53]. Although [HSO_3-BMIM][HSO_4] (an ionic liquid) was a relatively green and environmentally friendly homogeneous catalyst, it was viscous and expensive, and difficult to separate and recover from the reaction system [54]. In heterogeneous catalysts, $Sc(OTf)_3$ [55] had limitations such as long reaction time, low conversion rate and low yield. Furthermore, metal triploids were quite expensive, and their recovery was an obvious challenge. Although SAC-13 [56], Amberlyst 16 [57] and Zr–SBA-15(10)/[mim-ps]Cl–$ZnCl_2$ [58] showed certain catalytic activity in the esterification of HOAc and alcohols, their surfaces were all hydrophilic, and the catalysts would be deactivated due to the leaching of active components. In conclusion, the hydrophobic catalyst Fe_3O_4@SiO_2-Oc&$PrSO_3H$ prepared in this work has the advantages of high activity, strong stability and good reusability. Most importantly, it can be easily separated from the reaction system by an external magnet, and these characteristics are very applicable for the esterification reaction.

Table 4. Catalytic evaluation of different catalysts for esterification of HOAc and alcohols.

	Catalysts	Alcohol	T (°C)	t (h)	HOAc Conv. (%)	References
Homogeneous	H_2SO_4	Methanol	60	2	91.7	[52]
	Hydrogen iodide	Methanol	60	3	~53.13	[53]
	[HSO_3-BMIM][HSO_4]	N-butanol	75	3	75	[54]
	$Sc(OTf)_3$	Benzyl alcohol	20	48	98	[55]
Heterogeneous	SAC-13	Methanol	60	11	75	[56]
	Amberlyst 16	Ethanol	60	28	93.3	[57]
	Zr–SBA-15(10)/[mim-ps]Cl–$ZnCl_2$	Benzyl alcohol	100	5	93.6	[58]
	Fe_3O_4@SiO_2-Oc&$PrSO_3H$	Ethanol	80	3	88.57	this work

4. Conclusions

In brief, we successfully designed, prepared and characterized three novel magnetically-recoverable solid acid catalysts Fe_3O_4@SiO_2-Oc&$PrSO_3H$, Fe_3O_4@SiO_2-Me&$PrSO_3H$ and Fe_3O_4@SiO_2-$PrSO_3H$. The three catalysts were used in the synthesis of EAC to test their reactivity and stability, and the experimental results suggested that Fe_3O_4@SiO_2-Oc&$PrSO_3H$ with the strongest hydrophobicity had the highest HOAc conversion rate and water-

resistance. Under optimal reaction conditions (n_{EtOH}:n_{HOAc} = 6:1, 1 wt% catalyst loading, 80 °C, 3 h, 640 rpm), the conversion rate of HOAc reached the maximum of 88.57% with Fe_3O_4@SiO_2-Oc&PrSO_3H. In addition, the hydrophobic catalyst Fe_3O_4@SiO_2-Oc&PrSO_3H was easily separated under external magnetic conditions and its activity was not greatly reduced after repeating its use 6 times. These experimental results indicated that the catalyst had superior hydrophobicity and acidity balance, which allowed it to maintain high reactivity in an aqueous reaction system.

The novel solid acid catalysts prepared in this study are a kind of inorganic-organic hybrid material, and they realize the combination of inorganic supports with organic propylsulfonic acid groups and hydrophobic alkyl groups. At the same time, we could easily separate these catalysts from the reaction system by using their magnetic and heterogeneous properties. This approach will significantly reduce the cost of catalyst production and esterification reactions. More importantly, some studies have shown that these catalysts can not only be used in esterification reactions, but also can be applied to many other heterogeneous catalytic reactions in which water is a by-product.

Author Contributions: Conceptualization, Z.C.; methodology, J.S.; investigation, J.S. and J.L.; data curation, J.L.; writing—original draft preparation, J.L.; writing—review and editing, J.S.; supervision, Z.C. and B.Z. All authors have read and agreed to the published version of the manuscript.

Funding: The authors are grateful to the financial supports from the National Key R&D Program of China (No. 2019YFC1906705) and the National Natural Science Foundation of China (No. 21676085).

Institutional Review Board Statement: Not applicable.

Informed Consent Statement: Not applicable.

Data Availability Statement: All data collected in this study are contained within the article.

Conflicts of Interest: The authors declare no conflict of interest.

References

1. Rai, A.; Bhaskar, S.; Ganesh, K.M.; Ramamurthy, S.S. Cellphone-based attomolar tyrosine sensing based on Kollidon-mediated bimetallic nanorod in plasmon-coupled directional and polarized emission architecture. *Mater. Chem. Phys.* **2022**, *285*, 126129. [CrossRef]
2. Rai, A.; Bhaskar, S.; Reddy, N.; Ramamurthy, S.S. Cellphone-Aided Attomolar Zinc Ion Detection Using Silkworm Protein-Based Nanointerface Engineering in a Plasmon-Coupled Dequenched Emission Platform. *ACS Sustain. Chem. Eng.* **2021**, *9*, 14959–14974. [CrossRef]
3. Xu, X.; Geng, A.; Yang, C.; Carabineiro, S.A.C.; Lv, K.; Zhu, J.; Zhao, Z. One-pot synthesis of La–Fe–O@CN composites as photo-Fenton catalysts for highly efficient removal of organic dyes in wastewater. *Ceram. Int.* **2020**, *46*, 10740–10747. [CrossRef]
4. Zhang, C.; Yan, S.; Lin, J.; Hu, Q.; Zhong, J.; Zhang, B.; Cheng, Z. Electrochemical Reduction of CO_2 to CO on Hydrophobic Zn Foam Rod in a Microchannel Electrochemical Reactor. *Processes* **2021**, *9*, 1592. [CrossRef]
5. Shi, J.; Zhang, L.; Cheng, Z. Design of Water-Tolerant Solid Acids: A Trade-Off Between Hydrophobicity and Acid Strength and their Catalytic Performance in Esterification. *Catal. Surv. Asia* **2021**, *25*, 279–300. [CrossRef]
6. Xu, Z.; Zhao, G.; Hedin, N.; Xu, M.; Liu, J.; Ullah, L.; Zhang, S. Fast Catalytic Esterification Using a Hydrophobized Zr-MOF with Acidic Ionic Liquid Linkers. *Chemistryselect* **2020**, *5*, 1153–1156. [CrossRef]
7. Shu, Q.; Liu, X.; Huo, Y.; Tan, Y.; Zhang, C.; Zou, L. Construction of a Brönsted-Lewis solid acid catalyst La-PW-SiO_2/SWCNTs based on electron withdrawing effect of La(III) on π bond of SWCNTs for biodiesel synthesis from esterification of oleic acid and methanol. *Chin. J. Chem. Eng.* **2022**, *44*, 351–362. [CrossRef]
8. Durai, M.; Kumaravel, S.; Mukannan, A.; Krishnakumar, B.; Thiripuranthagan, S.; Ahn, Y.H. Esterification of valeric acid over PTA supported mesoporous Al-SBA-15 as efficient solid acid catalysts. *J. Porous Mater.* **2021**, *28*, 1907–1917. [CrossRef]
9. Liu, F.; Huang, K.; Zheng, A.; Xiao, F.-S.; Dai, S. Hydrophobic Solid Acids and Their Catalytic Applications in Green and Sustainable Chemistry. *ACS Catal.* **2018**, *8*, 372–391. [CrossRef]
10. Okuhara, T. Water-tolerant solid acid catalysts. *Chem. Rev.* **2002**, *102*, 3641–3666. [CrossRef]
11. Corma, A.; Garcia, H. Lewis acids: From conventional homogeneous to green homogeneous and heterogeneous catalysis. *Chem. Rev.* **2003**, *103*, 4307–4365. [CrossRef] [PubMed]
12. Zheng, A.; Liu, S.B.; Deng, F. ^{31}P NMR Chemical Shifts of Phosphorus Probes as Reliable and Practical Acidity. *Chem. Rev.* **2017**, *117*, 12475–12531. [CrossRef] [PubMed]
13. Choi, M.; Na, K.; Kim, J.; Sakamoto, Y.; Terasaki, O.; Ryoo, R. Stable single-unit-cell nanosheets of zeolite MFI as active and long-lived catalysts. *Nature* **2009**, *461*, 246–249. [CrossRef] [PubMed]

14. Suganuma, S.; Nakajima, K.; Kitano, M.; Yamaguchi, D.; Kato, H.; Hayashi, S.; Hara, M. Hydrolysis of Cellulose by Amorphous Carbon Bearing SO_3H, COOH, and OH Groups. *J. Am. Chem. Soc.* **2008**, *130*, 12787–12793. [CrossRef]
15. Zheng, A.; Li, S.; Liu, S.-B.; Deng, F. Acidic Properties and Structure–Activity Correlations of Solid Acid Catalysts Revealed by Solid-State NMR Spectroscopy. *Acc. Chem. Res.* **2016**, *49*, 655–663. [CrossRef]
16. Şimşek, V.; Şahin, S. Characterization and catalytic performance evaluation of a novel heterogeneous mesoporous catalyst for methanol–acetic acid esterification. *J. Porous Mater.* **2019**, *26*, 1657–1665. [CrossRef]
17. Liu, F.; Yi, X.; Chen, W.; Liu, Z.; Chen, W.; Qi, C.-Z.; Song, Y.-F.; Zheng, A. Developing two-dimensional solid superacids with enhanced mass transport, extremely high acid strength and superior catalytic performance. *Chem. Sci.* **2019**, *10*, 5875–5883. [CrossRef]
18. Polshettiwar, V.; Luque, R.; Fihri, A.; Zhu, H.; Bouhrara, M.; Basset, J.M. Magnetically recoverable nanocatalysts. *Chem. Rev.* **2011**, *111*, 3036–3075. [CrossRef]
19. Zheng, X.; Zhang, L.; Li, J.; Luo, S.; Cheng, J.-P. Magnetic nanoparticle supported polyoxometalates (POMs) via non-covalent interaction: Reusable acid catalysts and catalyst supports for chiral amines. *Chem. Commun.* **2011**, *47*, 12325–12327. [CrossRef]
20. Zuo, B.; Li, W.; Wu, X.; Wang, S.; Deng, Q.; Huang, M. Recent Advances in the Synthesis, Surface Modifications and Applications of Core-Shell Magnetic Mesoporous Silica Nanospheres. *Chem. Asian. J.* **2020**, *15*, 1248–1265. [CrossRef]
21. Hubetska, T.; Kobylinska, N.; Menendez, J. Application of Hydrophobic Magnetic Nanoparticles as Cleanup Adsorbents for Pesticide Residue Analysis in Fruit, Vegetable, and Various Soil Samples. *J. Agric. Food Chem.* **2020**, *68*, 13550–13561. [CrossRef]
22. Cardoso, V.F.; Francesko, A.; Ribeiro, C.; Bañobre-López, M.; Martins, P.; Lanceros-Mendez, S. Advances in Magnetic Nanoparticles for Biomedical Applications. *Adv. Healthc. Mater.* **2018**, *7*, 1700845. [CrossRef] [PubMed]
23. Bhaskar, S.; Rai, A.; Kalathur Mohan, G.; Ramamurthy, S.S. Mobile Phone Camera-Based Detection of Surface Plasmon-Coupled Fluorescence from Streptavidin Magnetic Nanoparticles and Graphene Oxide Hybrid Nanointerface. *ECS Trans.* **2022**, *107*, 3223–3232. [CrossRef]
24. Li, S.; Wang, W.; Zhao, J. Magnetic-heteropolyacid mesoporous catalysts for deep oxidative desulfurization of fuel: The influence on the amount of APES used. *J. Colloid Interface Sci.* **2020**, *571*, 337–347. [CrossRef] [PubMed]
25. Zhang, Q.; Su, H.; Luo, J.; Wei, Y. A magnetic nanoparticle supported dual acidic ionic liquid: A "quasi-homogeneous" catalyst for the one-pot synthesis of benzoxanthenes. *Green Chem.* **2012**, *14*, 201–208. [CrossRef]
26. Shylesh, S.; Schünemann, V.; Thiel, W.R. Magnetically Separable Nanocatalysts: Bridges between Homogeneous and Heterogeneous Catalysis. *Angew. Chem. Int. Ed.* **2010**, *49*, 3428–3459. [CrossRef] [PubMed]
27. Tartaj, P.; Serna, C.J. Synthesis of Monodisperse Superparamagnetic Fe/Silica Nanospherical Composites. *J. Am. Chem. Soc.* **2003**, *125*, 15754–15755. [CrossRef]
28. Graf, C.; Vossen, D.L.J.; Imhof, A.; van Blaaderen, A. A General Method To Coat Colloidal Particles with Silica. *Langmuir* **2003**, *19*, 6693–6700. [CrossRef]
29. El-Toni, A.M.; Habila, M.A.; Labis, J.P.; Alothman, Z.A.; Alhoshan, M.; Elzatahry, A.A.; Zhang, F. Design, synthesis and applications of core–shell, hollow core, and nanorattle multifunctional nanostructures. *Nanoscale* **2016**, *8*, 2510–2531. [CrossRef]
30. Lu, A.H.; Salabas, E.L.; Schüth, F. Magnetic nanoparticles: Synthesis, protection, functionalization, and application. *Angew. Chem. Int. Ed.* **2007**, *46*, 1222–1244. [CrossRef] [PubMed]
31. Wu, Z.; Li, Z.; Wu, G.; Wang, L.; Lu, S.; Wang, L.; Wan, H.; Guan, G.J.I.; Research, E.C. Brønsted Acidic Ionic Liquid Modified Magnetic Nanoparticle: An Efficient and Green Catalyst for Biodiesel Production. *Ind. Eng. Chem. Res.* **2014**, *53*, 3040–3046. [CrossRef]
32. Zhang, H.; Li, H.; Pan, H.; Wang, A.; Souzanchi, S.; Xu, C.; Yang, S. Magnetically recyclable acidic polymeric ionic liquids decorated with hydrophobic regulators as highly efficient and stable catalysts for biodiesel production. *Appl. Energy* **2018**, *223*, 416–429. [CrossRef]
33. Xie, W.; Wang, H. Immobilized polymeric sulfonated ionic liquid on core-shell structured Fe_3O_4/SiO_2 composites: A magnetically recyclable catalyst for simultaneous transesterification and esterifications of low-cost oils to biodiesel. *Renew. Energy* **2020**, *145*, 1709–1719. [CrossRef]
34. Escobar, A.M.; Blanco, M.N.; Martínez, J.J.; Cubillos, J.A.; Romanelli, G.P.; Pizzio, L.R. Biomass Derivative Valorization Using Nano Core-Shell Magnetic Materials Based on Keggin-Heteropolyacids: Levulinic Acid Esterification Kinetic Study with N-Butanol. *J. Nanomater.* **2019**, *2019*, 5710708. [CrossRef]
35. Abida, K.; Chudasama, B.; Ali, A. Development and functionalization of magnetic nanoparticles as stable and reusable catalysts for triacetin synthesis. *New J. Chem.* **2020**, *44*, 9365–9376. [CrossRef]
36. Nuryono, N.; Qomariyah, A.; Kim, W.; Otomo, R.; Rusdiarso, B.; Kamiya, Y. Octyl and propylsulfonic acid co-fixed Fe_3O_4@SiO_2 as a magnetically separable, highly active and reusable solid acid catalyst in water. *Mol. Catal.* **2019**, *475*, 110248. [CrossRef]
37. Esfahani, F.K.; Zareyee, D.; Yousefi, R. Sulfonated Core-Shell Magnetic Nanoparticle (Fe_3O_4@SiO_2@$PrSO_3H$) as a Highly Active and Durable Protonic Acid Catalyst; Synthesis of Coumarin Derivatives through Pechmann Reaction. *ChemCatChem* **2014**, *6*, 3333–3337. [CrossRef]
38. Mobaraki, A.; Movassagh, B.; Karimi, B. Hydrophobicity-enhanced magnetic solid sulfonic acid: A simple approach to improve the mass transfer of reaction partners on the surface of the heterogeneous catalyst in water-generating reactions. *Appl. Catal. A Gen.* **2014**, *472*, 123–133. [CrossRef]

39. Liu, F.; Kong, W.; Qi, C.; Zhu, L.; Xiao, F.-S. Design and Synthesis of Mesoporous Polymer-Based Solid Acid Catalysts with Excellent Hydrophobicity and Extraordinary Catalytic Activity. *ACS Catal.* **2012**, *2*, 565–572. [CrossRef]
40. Long, W.; Jones, C. Hybrid Sulfonic Acid Catalysts Based on Silica-Supported Poly(Styrene Sulfonic Acid) Brush Materials and Their Application in Ester Hydrolysis. *ACS Catal.* **2011**, *1*, 674–681. [CrossRef]
41. Tsai, C.-H.; Chen, H.-T.; Althaus, S.M.; Mao, K.; Kobayashi, T.; Pruski, M.; Lin, V.S.Y. Rational Catalyst Design: A Multifunctional Mesoporous Silica Catalyst for Shifting the Reaction Equilibrium by Removal of Byproduct. *ACS Catal.* **2011**, *1*, 729–732. [CrossRef]
42. Duan, X.; Liu, Y.; Zhao, Q.; Wang, X.; Li, S. Water-tolerant heteropolyacid on magnetic nanoparticles as efficient catalysts for esterification of free fatty acid. *RSC Adv.* **2013**, *3*, 13748–13755. [CrossRef]
43. Zolfagharinia, S.; Kolvari, E.; Koukabi, N. A New Type of Magnetically-Recoverable Heteropolyacid Nanocatalyst Supported on Zirconia-Encapsulated Fe_3O_4 Nanoparticles as a Stable and Strong Solid Acid for Multicomponent Reactions. *Catal. Lett.* **2017**, *147*, 1551–1566. [CrossRef]
44. Kuzminska, M.; Carlier, N.; Backov, R.; Gaigneaux, E.M. Magnetic nanoparticles: Improving chemical stability via silica coating and organic grafting with silanes for acidic media catalytic reactions. *Appl. Catal. A Gen.* **2015**, *505*, 200–212. [CrossRef]
45. Li, J.; Zhao, H.; Hou, X.; Fa, W.; Cai, J. Fe_3O_4@SiO_2-SO_3H nanocomposites: An efficient magnetically separable solid acid catalysts for esterification reaction. *Micro Nano Lett.* **2017**, *12*, 53–57. [CrossRef]
46. Wang, C.; Tao, S.; Wei, W.; Meng, C.; Liu, F.; Han, M. Multifunctional mesoporous material for detection, adsorption and removal of Hg^{2+} in aqueous solution. *J. Mater. Chem.* **2010**, *20*, 4635–4641. [CrossRef]
47. Ghasemzadeh, M.A.; Abdollahi-Basir, M.H.; Babaei, M. Fe_3O_4@SiO_2–NH_2 core-shell nanocomposite as an efficient and green catalyst for the multi-component synthesis of highly substituted chromeno[2,3-b]pyridines in aqueous ethanol media. *Green Chem. Lett. Rev.* **2015**, *8*, 40–49. [CrossRef]
48. Sharma, P.; Vyas, S.; Patel, A. Heteropolyacid supported onto neutral alumina: Characterization and esterification of 1° and 2° alcohol. *J. Mol. Catal. A Chem.* **2004**, *214*, 281–286. [CrossRef]
49. Liu, F.; Wang, L.; Sun, Q.; Zhu, L.; Meng, X.; Xiao, F.-S. Transesterification Catalyzed by Ionic Liquids on Superhydrophobic Mesoporous Polymers: Heterogeneous Catalysts That Are Faster than Homogeneous Catalysts. *J. Am. Chem. Soc.* **2012**, *134*, 16948–16950. [CrossRef]
50. Manayil, J.C.; dos Santos, V.C.; Jentoft, F.C.; Granollers Mesa, M.; Lee, A.F.; Wilson, K. Octyl Co-grafted $PrSO_3H$/SBA-15: Tunable Hydrophobic Solid Acid Catalysts for Acetic Acid Esterification. *ChemCatChem* **2017**, *9*, 2231–2238. [CrossRef]
51. Dacquin, J.-P.; Cross, H.E.; Brown, D.R.; Düren, T.; Williams, J.J.; Lee, A.F.; Wilson, K. Interdependent lateral interactions, hydrophobicity and acid strength and their influence on the catalytic activity of nanoporous sulfonic acid silicas. *Green Chem.* **2010**, *12*, 1383–1391. [CrossRef]
52. Mekala, M.; Goli, V.R. Kinetics of esterification of methanol and acetic acid with mineral homogeneous acid catalyst. *Chin. J. Chem. Eng.* **2015**, *23*, 100–105. [CrossRef]
53. Rönnback, R.; Salmi, T.; Vuori, A.; Haario, H.; Lehtonen, J.; Sundqvist, A.; Tirronen, E. Development of a kinetic model for the esterification of acetic acid with methanol in the presence of a homogeneous acid catalyst. *Chem. Eng. Sci.* **1997**, *52*, 3369–3381. [CrossRef]
54. He, R.; Zou, Y.; Muhammad, Y.; Tong, Z. Study on the Intensification of Reaction Kinetics and Reactive Distillation for the Esterification of N-Butyl Acetate Using [HSO_3-BMIM][HSO_4] as a High-Efficiency Ionic Liquid Catalyst. *Ind. Eng. Chem. Res.* **2021**, *60*, 12847–12863. [CrossRef]
55. Lee, S.-G.; Park, J.H. Metallic Lewis acids-catalyzed acetylation of alcohols with acetic anhydride and acetic acid in ionic liquids: Study on reactivity and reusability of the catalysts. *J. Mol. Catal. A Chem.* **2003**, *194*, 49–52. [CrossRef]
56. Liu, Y.; Lotero, E.; Goodwin, J.G. A comparison of the esterification of acetic acid with methanol using heterogeneous versus homogeneous acid catalysis. *J. Catal.* **2006**, *242*, 278–286. [CrossRef]
57. Avhad, M.R.; Osborg, M.V.; Marchetti, J.M. Reusable Amberlyst 16 catalyst for acetic acid esterification relevant for pyrolysis bio-oil upgrading process. *React. Kinet. Mech. Catal.* **2019**, *126*, 181–197. [CrossRef]
58. Dai, L.; Zhao, Q.; Fang, M.; Liu, R.; Dong, M.; Jiang, T. Catalytic activity comparison of Zr–SBA-15 immobilized by a Brønsted–Lewis acidic ionic liquid in different esterifications. *RSC Adv.* **2017**, *7*, 32427–32435. [CrossRef]